Chapter 6
Non-contact Friction

Marcin Kisiel, Markus Samadashvili, Urs Gysin and Ernst Meyer

Abstract Our understanding of friction and mechanism of energy dissipation has undoubtedly experienced a tremendous profit after the introduction of scanning probe microscopy. Nowadays the tribological response of a sliding asperity can be easily traced down to the atomic scale. Still, many important aspects of friction on the nanoscale are scarcely studied. Among them we can easily recognize the dissipation accompanying the motion of a nano-object in close proximity to a solid surface. An example, which is quite suitable for experimental investigations, is given by the oscillations of a tiny pendulum. Here we report on different mechanisms of energy loss—for instance probably the most common Joule dissipation. Next we demonstrate that pendulum oscillations are expected to induce both phononic and electronic excitations in the underlying surface and the clear distinction between them is possible while working over metal/superconductor phase transition. Finally, we describe an example of coupling of mechanical oscillator to the charge-density-wave phase, an exquisitely subtle long-range order property of matter.

6.1 Introduction: Dissipation at Large Separation

Friction force has a pivotal role in nature and our everyday life is full of examples of frictional processes. When two macroscopic bodies slide in contact energy is dissipated due to friction [1, 2]. Sometimes it is desired, like in case of brakes in the bicycle, sometimes unwelcome—when you ask yourself why your automated coffee machine broke for the third time. In nanoscale, a tiny friction force is present

M. Kisiel (✉) · M. Samadashvili · U. Gysin · E. Meyer
Department of Physics, Univeristy of Basel, Klingelberstrasse 82,
4056 Basel, Switzerland
e-mail: marcin.kisiel@unibas.ch

M. Samadashvili
e-mail: Markus.Langer@unibas.ch

U. Gysin
e-mail: urs.gysin@unibas.ch

E. Meyer
e-mail: ernst.meyer@unibas.ch

S. Morita et al. (eds.), *Noncontact Atomic Force Microscopy*,
NanoScience and Technology, DOI 10.1007/978-3-319-15588-3_6

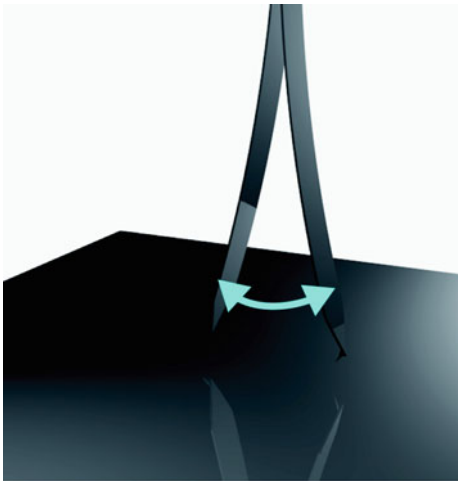

Fig. 6.1 Schematic view of the oscillating cantilever in the pendulum geometry

when bodies in relative motion are separated by few nanometer gap [3–5]. This non-contact form of friction might be successfully measured by highly sensitive cantilever oscillating like a tiny pendulum over the surface as it is shown in Fig. 6.1 [5–8]. The elusive non-contact friction might by due to vdW interaction, which is mediated by the long-range electromagnetic fields or in many cases by fluctuations of static surface charges arising from material inhomogeneities [9]. It also strongly depends on the bias voltage between tip and sample. The non-contact friction or we should rather say energy dissipation is a non-reversible process, where the kinetic energy of the damped oscillator is transferred into heat, which is observed as a decay in time of the cantilever amplitude. The amplitude drops until the thermal equilibrium is reached. Both decay time τ and equilibrium fluctuations $x(t)$ contain information about the dissipative process. The quality factor Q is equal to:

$$Q = \frac{\tau \omega_0}{2} \tag{6.1}$$

and the corresponding damping coefficient is given by:

$$\Gamma = \frac{k}{\omega_0 Q} \tag{6.2}$$

where k is the spring constant and ω_0 is oscillation frequency of the cantilever. It is obvious (6.2), that the smallest spring constant k and the highest quality factor Q imply higher non-contact friction sensitivity. Cantilevers with these features are also very force sensitive. The minimal detectable force $F_{\min}$ is given by the formula:

$$F_{\min} = \sqrt{\frac{2k_B T \Gamma \Delta\omega}{\pi}} \tag{6.3}$$

where k_B is the Boltzmann constant, T and $\Delta\omega$ are the temperature and the bandwidth of the measurement. Any change of the friction coefficient Γ is always accompanied by a change of the minimal detectable force.

In case of an extremely soft cantilever characterised by spring constant $k = 130\,\mu$N/m, the quality factor $Q = 250{,}000$ and the resonance frequency $f_0 = 6\,$kHz the non-contact friction is in the order of $\Gamma = 10^{-14}\,$kg/s.

Approaching soft cantilever to the surface will open new dissipation channels, however the tip-surface interaction will immediately provoke cantilever snap into contact. That will happen on every surface when the attractive force gradient is larger then cantilever spring constant. An easy way to overcome this obstacle is to oscillate the cantilever in a pendulum geometry. This way the cantilever is oriented perpendicularly to the surface and oscillates like a tiny pendulum over it.

In this chapter several experiments reporting on non-contact friction are discussed. Next section concerns the experimental tool designed to study non-contact friction—the Atomic Force Microscope (AFM) operating in pendulum geometry. We next discuss the mechanisms influencing internal dissipation of the sensor, as they strongly limit our measurement sensitivity. In order to introduce non-contact friction itself, few mechanisms leading to this phenomena are discussed in the following section. Finally three experiments dealing with non-contact friction are reported. This part is structured as follows: first, experiment on γ-irradiated quartz sample is discussed. It was found that non-contact friction increases at separations of 30 nm. In this case long-range dissipation is related to the long-range electrostatic forces and distance dependence of the contact potential was found to influence the non-contact friction. Next we discuss the experiment on superconducting Nb surface which allowed to distinguish between electronic and phononic dissipation channels. The last part reports on experiment on $NbSe_2$ surface, where the non-contact friction is caused by the hysteretic switching of the charge density wave provoked by the oscillating tip.

6.2 The Pendulum AFM System

6.2.1 The Microscope

The results reported in this chapter were obtained by means of pendulum AFM located at University of Basel with the capability of working under Ultra High Vacuum (UHV) ($p < 10^{-10}\,$mbar) as well as cryogenic conditions ($T = 5\,$K). The setup of the microscope is shown in Fig. 6.2 and is described in details elsewhere [10].

It is worth to mention that the beam deflection detection technique [11] was chosen to measure the cantilever oscillations. The technique does not rely on a laser light source with a long coherence length. Instead superluminescent diodes (e.g. Superlum SLD-381-MP3 or Hamamatsu SLD) with lower noise levels are used as a light source. The cantilever motion is controlled by means of standard Phase-Lock-Loop (PLL) electronics where the detection of the frequency, amplitude and phase are performed.

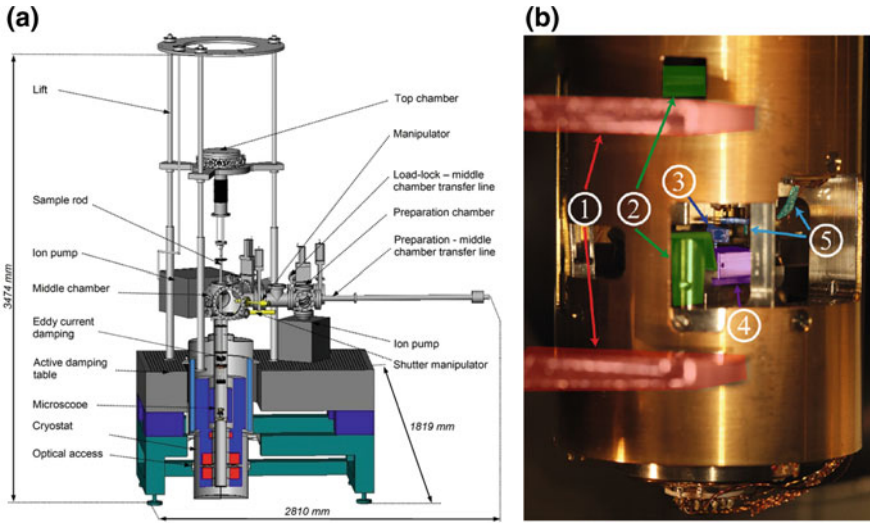

Fig. 6.2 The UHV system is shown in figure (**a**) with the top loaded cryostat. The microscope itself is shown in (**b**), where *1* (*red*) is the microscope holder, *2* (*green*) the mirrors of the beam deflection detection system, *3* (*dark blue*) the cantilever itself, *4* (*violet*) the sample holder and *5* (*light blue*) the STM shielded current line

In order to maintain the amplitude of oscillation constant the excitation voltage is brought back to the shaking piezo.

The pendulum AFM is not an overwhelming imaging tool and the atomic resolution is hard to reach. The capability to acquire a topography information is limited due to the lateral oscillation and the spacial averaging is performed in every topographic pixel. The strength of the pendulum geometry lays in the spectroscopy.

6.2.2 Internal Friction of the Cantilever

The experimentally determined cantilever damping Γ is a superposition of different ingredients:

$$\Gamma(T, p, E, B, d, ...) = \Gamma_0 + \Gamma_{TS} \tag{6.4}$$

and depends in general on temperature T, pressure p and external electric E and magnetic B fields. The influence of the electromagnetic field plays a role in case of tip-sample proximity. This effect leads to a distance dependent friction coefficient $\Gamma_{TS}(d)$ at small tip sample separations [5–7, 12–14]. The internal friction of the cantilever Γ_0 describes the friction losses which occur while bending of the cantilever and several components might be distinguished:

1. Viscous damping due to the presence of gases,
2. Energy losses due to clamping of the cantilever,

3. Thermoelastic damping,
4. Bulk and surface energy looses.

To minimize the viscous damping which occurs due to inelastic scattering between the vibrating cantilever and gas molecules cantilever has to be operated under vacuum conditions. At pressures below $p < 10^6$ mbar viscous damping is negligible [15]. The second effect might be partly eliminated by means of rigid clamping and avoiding of glues with high damping rates [16].

Periodic compression and expansion of oscillating cantilever causes heat flow between compressed and expanded areas. The energy loss due to local heating of the cantilever is known as a thermoelastic damping. The thermoelastic damping is the dominant loss mechanism at room temperature [17]. At temperatures below $T < 200$ K other mechanisms start to dominate such as bulk or surface losses.

Bulk and surface losses due to scattering of elastic waves on defects present on the surface or in the bulk are dominant loss mechanisms at low temperatures. The time dependent stress field changes the energy landscape of the defects and the instabilities of those might occur. The effect is related to jumps of the atoms between different equilibrium positions. This effect is temperature dependent and dissipation versus temperature curves show Debye activation peaks. In case of Silicon cantilever Debye peak is observed often at $T = 30$ K [18]. Another peak positioned at $T = 160$ K cannot be related to such an activation peak because of too high activation barrier. It is also observed that the peak does not shift with the resonance frequency, which is not in agreement with the simple activation energy model. It has been observed that the 160 K peak is reduced after annealing the cantilever under vacuum conditions and the authors suggest that it is related to an existence of adsorbate layer [18]. In fact coating of cantilevers leads to a strong increase of dissipation. The rise of Γ_0 is owing to the phonon scattering on grain boundaries because of polycrystalline nature of the coating layer. The presence of adsorbates (H_2O or hydrocarbons) also have a negative impact on the internal friction. It has been shown that annealing at temperatures up to about 700 °C under ultra high vacuum conditions leads to substantial reduction of dissipation [19, 20]. Figure 6.3 demonstrates the improvement of pristine quality

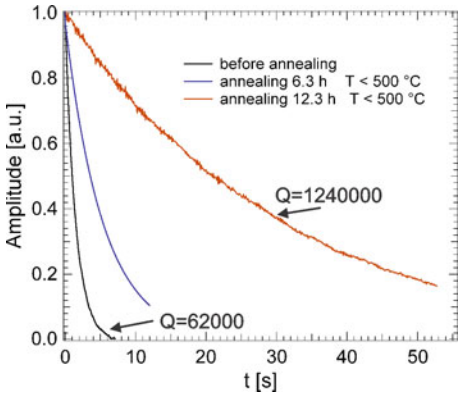

Fig. 6.3 Ring down measurement of a cantilever before and after annealing under UHV-conditions and at the temperature $T = 77$ K. The initial quality factor of 62,000 is improved by an order of magnitude after 6 h annealing. Further annealing improved the quality factor to 1,240,000. Data from [20]

factor of 62,000 by an order of magnitude after 6 h annealing at temperatures below at 500 °C. Further annealing improved the quality factor to 1,200,000 as measured in $T = 77$ K. The increase of sensitivity is mainly due to removal of weakly bounded molecules from the cantilever surface or alternatively the amount of surface/bulk defects is reduced. It is also known that long term annealing leads to negligible amount of localized charges at the end of the probing tip.

6.3 Non-contact Friction Due to Tip-Sample Interaction

Approaching the cantilever close to a surface leads to distance d dependent dissipation $\Gamma_{TS}(d)$. Experimentally there are three methods to determine the non-contact friction: ring-down measurements, the measurement of the excitation voltage A_{exc} which is needed to maintain constant amplitude of oscillation and the measurement of the power spectral density $S(\omega)$ of the cantilever fluctuations [6, 21].

In the first method the Γ is determined from the decay time τ of the cantilever oscillations using the relations (6.1) and (6.2). In this method, the cantilever is oscillating at its resonant frequency with a constant amplitude until the driving voltage A_{exc} is suddenly switched off and the oscillations decay towards thermal equilibrium with a characteristic time τ (see Fig. 6.3). This method apply to the sensors with relatively large quality factors Q.

Usually the cantilever oscillations are controlled by means of phase-locked loop (PLL) feedback system, where the phase between constant amplitude cantilever oscillation signal and cantilever excitation A_{exc} is locked. This way the frequency shift Δf caused by the tip sample interaction is measured. The friction coefficient is calculated according to a formula:

$$\Gamma = \Gamma_0 \left(\frac{A_{\mathrm{exc}}(d)}{A_{\mathrm{exc},0}} - \frac{f(d)}{f_0} \right) , \tag{6.5}$$

where Γ_0 is the internal cantilever dissipation, measured at large tip-sample separation, $A_{\mathrm{exc}}(d)$ and $f(d)$ are the distance dependent excitation amplitude (as measured by the excitation voltage needed to excite the cantilever at constant oscillation amplitude A) and frequency of the cantilever and the suffix zero refers to the free cantilever. Both methods are complementary as it is demonstrated in Fig. 6.4.

Quantities like the frequency noise $\delta\omega$ of cantilever which oscillates with an amplitude x_0 at its resonance frequency ω_0 depend on the dissipation Γ [21]:

$$\delta\omega = \frac{\omega}{x_0 k} \sqrt{\frac{2 k_B T \Gamma \Delta\omega}{\pi^3}} \tag{6.6}$$

The oscillator frequency noise $\delta\omega$ is influenced by Γ and the temperature T. It is therefore possible to quantitatively measure the non-contact friction based on power

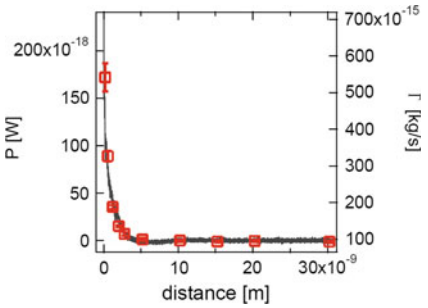

Fig. 6.4 The non-contact friction coefficient Γ and dissipated power P as a function of distance from Cu(110) surface measured by means of ring down method (*red squares*) and by measurement of the excitation voltage A_{exc} (*gray line*), (6.5). Cantilever and sample temperature was equal $T = 77\,\mathrm{K}$

spectral density of the $\delta\omega$. The power spectral noise density $S(\omega)^2\Delta\omega = \delta\omega^2$ can be estimated in a narrow bandwidth as follows:

$$S(\omega)^2 = \frac{2k_bT\omega_0^2\Gamma}{\pi^3k^2x_0^2} \tag{6.7}$$

6.4 Origins of Non-contact Friction

When contact friction deals with two bodies being close enough to interact chemically, the non-contact energy dissipation appears at any distance larger than chemical interaction range. The range of the interacting force determines the distance dependency of the friction coefficient Γ_{TS} and thus it is possible to distinguish between long-range and short-range friction forces. The non-contact friction mechanisms are still the subject of ongoing discussion, since the theoretically predicted values [3, 4] might be sometimes orders of magnitude smaller than experimentally observed ones [5, 6, 14, 22]. An overview of main dissipation mechanisms is presented below.

6.4.1 Phononic Friction

The non-contact friction by phonon creation of two interacting surfaces is only observed for realtively small tip sample separations, when the force acting on the surface is large. It implies the existence of tiny deformation of the surfaces induced by attractive van der Waals or electrostatic interaction. The oscillating cantilever tip over the surface of an elastic body might create the the time dependent stress field and thus excites acoustic waves parallel to the surface. In this case the energy is dissipated into emission of acoustic phonons. The situation is schematically sketched in Fig. 6.5a [23].

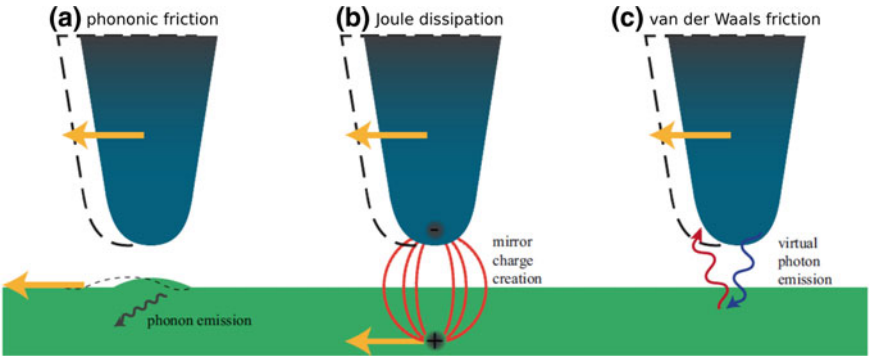

Fig. 6.5 Phononic friction appears at small tip sample separation. A surface deformation occurs and is dragged along with the tip movement. Upon the spatial variation of this deformation phonons are created and energy loss occurs (**a**). Joule dissipation takes place if non compensated charges situated on the surface or on the tip move through resistive media. The spatial variation creates a displacement current in tip/sample and the energy is lost to Joule heating (**b**). The van der Waals friction arises from the van der Waals force owing to dipole fluctuations or random currents. This is equivalent to emission of real/virtual photon to the surface. The re-emitted photon is absorbed back in the tip. The friction arises due to the fact, that the initial photon compared the the reabsorbed one are Doppler shifted (**c**)

6.4.2 Joule Dissipation

The Joule dissipation is present due to electrostatic forces which arise from permanent or fluctuating charges situated on the tip or/and the surface. The charge induced on the other surface follows the tip motion and experiences a resistive loss [13]. The charge interaction is strongly enhanced by biasing a tip. If a voltage U is applied between tip and sample, the system acts as a distance dependent capacitance. Due to the amplitude x_0 of the driven oscillator, the capacitance varies accordingly. The change of capacitance generates an alternating displacement current in the tip or sample upon the oscillation at the driving frequency ω_0. The dynamic distance is then given by $z(t) = z_0 + x_0 \cos(\omega_0 t)$. Further, we can write the displacement current D as:

$$D(t) = \frac{\partial C}{\partial t} U = \frac{\partial C}{\partial z} \frac{\partial z}{\partial t} U \tag{6.8}$$

and the dissipated power:

$$P_{\text{Joule}} = R_{t-s} D^2(t) = R_{t-s} \left(\frac{\partial C}{\partial z} \right)^2 U^2 x_0^2 \omega_0^2 \sin^2(\omega_0 t) \tag{6.9}$$

where R_{t-s} is the electrical resistance of the tip and sample. The average power dissipated $\langle P_{\text{Joule}} \rangle$ in one single oscillation cycle is equal:

$$\langle P_{\text{Joule}} \rangle = \pi R_{t-s} \left(\frac{\partial C}{\partial z} \right)^2 U^2 x_0^2 \omega_0^2 \tag{6.10}$$

6.4.3 van der Waals Friction

The van der Waals friction is a dissipative analogue of the conservative van der Waals force. Both mechanisms rely on the same physics. The force arises from the quantum fluctuation of the electron density, when a spontaneous dipole is created. The short lived dipole interacts with a nearby surface via a photon exchange and induces a dipole moment. The induced dipole re-emits a photon to the original one and a force arises between the two dipoles. When two bodies are in relative motion with respect to each other the friction force occurs owing to the Doppler shift of the exchanged photon. The situation is shown in Fig. 6.5c. The calculation of the van der Waals friction is more complex than the force, since it originates from the electromagnetic field fluctuations with moving boundary conditions. The literature approaches the solution by regarding each surface in its reference frame. The relation between the two electromagnetic fields of each reference frame is determined by the Lorentz transformation [3, 4]. Since, Γ originates from the stochastic electromagnetic field fluctuations, the energy loss might be calculated by means of fluctuation-dissipation theorem [24, 25]. For non-contact friction coefficient we obtain:

$$\Gamma \propto \frac{1}{k_B T} \int_0^\infty \langle \mathbf{f}(t_0) \mathbf{f}(t_1) \rangle \tag{6.11}$$

where $\mathbf{f}(t)$ is random force which obeys $\langle \mathbf{f}(t) \rangle = 0$ and $\langle \mathbf{f}(t_0) \mathbf{f}(t_1) \rangle$ is the autocorrelation function of the random force. The theory of van der Waals friction is more complex than conservative van der Waals force and up to now there is no unified understanding of it. Many theories [3, 26–28] lead to different scaling laws and large differences in the magnitude of the friction force. Experimentally, the problem is challenging, as well. Stipe and co-workers probably came closest to measuring the tiny vdW friction [5].

6.5 Dissipation at Large Separation

Dissipation due to electromagnetic interaction was first observed by Denk and Pohl [13]. Subsequent measurements [5] showed substantial electrostatic dissipation at separations of 1–200 nm measured by means of ultrasensitve force sensors oscillating in pendulum geometry. Friction coefficients of the order of 10^{-13} kg/s between gold coated tip and metal substrate were reported. The distance dependence of the friction coefficient scales with a power law $\Gamma \propto d^{-n}$ with an exponent $n = 1.3$. Volokitin et al. [3, 4] have found those data consistent with dissipation between a spherical

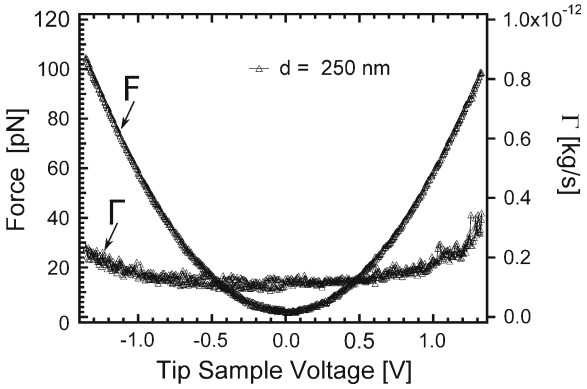

Fig. 6.6 Voltage-dependence of the normal force (F) and friction coefficient (Γ) at tip distance of d = 250 nm from 20 nm thick gold film. The quadratic behaviour of the normal force and the friction coefficient with respect to bias voltage indicate that non-contact friction has electrostatic origin. Data from [20]

tip and the clean metal surface. Their calculation showed that dissipation caused by fluctuations of the contact potential scales with the exponent $n = 1.5$.

Rast and collaborators performed similar experiment under ultra high vacuum conditions and at temperature $T = 7$ K [20]. They used a magnetic Co-Sm tip oscillating in proximity of γ-irradiated quartz substrate coated subsequently with 20 nm of gold. As it is shown in Fig. 6.6 both conservative and dissipative forces increase and obey the parabolic behaviour when the bias voltage is applied. The quadratic behaviour of Γ versus bias voltage is direct evidence of the electronic origin of friction [3–5]. In this particular case the time dependent electric field induces local electric currents in the sample and/or the cantilever. Moreover, the authors noticed strong dependence of contact potential on distance, presumably due to tip averaging over areas with different work functions. Both non-contact friction and force have a minimum exactly when the contact potential between tip and sample is compensated i.e. $V = +20$ mV, therefore it is important to compensate the contact potential in order to establish the minimum friction coefficients.

Compensating the contact potential allows us to investigate the friction force which is not dominated by Joule losses. Figure 6.7 shows the distance d dependence of the friction coefficient as a function of distance with compensated contact potential. Absolute values are between 1×10^{-13} kg/s down to 5×10^{-14} kg/s at $d > 30$ nm where the dissipation is mainly governed by internal friction. At separations below 30 nm the friction coefficient is larger than the internal friction of the cantilever and non-reversible energy flow between tip and sample is observed. Volokitin et al. [3, 4] calculated the friction coefficient of a tip separated by a distance d generated by a van der Waals friction force in dielectrics. For a cylindrical tip with radius R and width w the calculated friction coefficient scales with $d^{-1/2}$, which is in good agreement with the data. The friction might then occur due to fluctuating defects

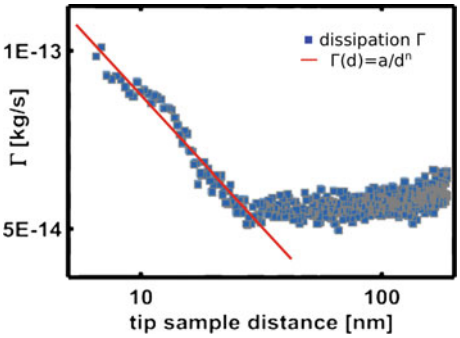

Fig. 6.7 Distance dependence of the non-contact friction coefficient for compensated contact potential at separations between 1–100 nm. At distance up to 30 nm friction scales with inverse power law $\Gamma \propto d^{-n}$. At a separation larger than 30 nm the friction is governed by the internal friction Γ_0 of the cantilever. Temperature of the measurement $T = 7$ K. Data from [20]

in the quartz crystal. The higher the defect concentration the higher the value of distance dependent friction coefficient. However, the 20 nm thick gold film prevents a penetrating of the electrical field into the nonconducting substrate, so that damping effects by this mechanism are minimized. A metal film always consists of a number of crystallites whose work function depend of the crystal orientation. The magnet tip also consists of numerous of crystals. Electrical fields always exist between the crystal boundaries with different work function. and the external bias voltage never compensates globally the electrical field. The non compensated electrical fields are decisive for the friction losses.

6.6 Suppression of Electronic Friction in the Superconducting State

The pendulum AFM tip oscillating in close proximity to a substrate might induce phononic excitations. An easy way to distinguish between electronic and phononic contribution to non-contact friction is to work across the metal/superconductor transition. In order to estimate the phononic and electronic contributions, Kisiel et al. [6] oscillate the pendulum cantilever over a 150 nm thick Nb film. The ultrasensitive cantilever with spring constant $k = 30$ mN/m and resonance frequency $f = 5.3$ kHz was used. After long term annealing under UHV condition the internal dissipation was improved and equal to $\Gamma_0 = 2.0 \times 10^{-12}$ kg/s at temperature $T = 6$ K. The cantilever end was exposed to focus ion beam (FIB) to form a sharp tip with spherical apex, approximately 50 nm in diameter (inset in Fig. 6.8). The oscillation amplitude $A = 5$ nm was kept constant during the measurement.

The dependence of the friction coefficient on the temperature is shown in Fig. 6.8. During the measurement the tip sample distance d $= 0.5$ nm was kept constant and

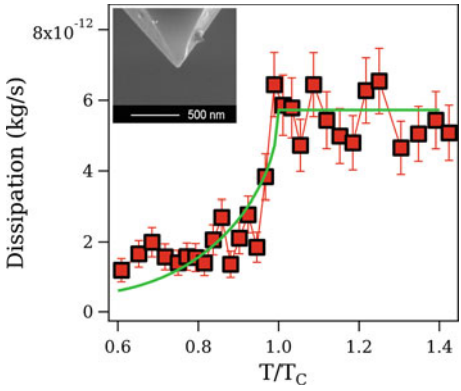

Fig. 6.8 Temperature variation of the non-contact friction coefficient across $T_c = 9.2\,\mathrm{K}$ of Nb surface. The *green line* is a fit of (6.12) to the measured data. *Inset* the focused ion beam (FIB) shaped tip used in experiment

the contact potential between tip and sample was compensated. The non-contact friction was measured by means of ring down method (see Fig. 6.3). The non-contact friction coefficient rises by a factor of three when the critical temperature T_c is approached from below and levels off in the normal state. It is equal to 25 μeV/cycle in superconducting phase and rises to 80 μeV/cycle in a metallic phase. The character of the friction coefficient in the vicinity of $T_c = 9.2\,\mathrm{K}$ is smooth as predicted by BCS (Bardeen-Cooper-Schrieffer) theory of superconductivity [29]. Persson [30, 31] realized that friction over superconducting phase transition is owing to the acoustic attenuation of the longitudinal acoustic phonons known from BCS theory. The surface contribution to the friction is given by temperature dependent formula:

$$\frac{\Gamma_{\mathrm{surf}}(T)}{\Gamma_{\mathrm{surf}}(T_c)} \simeq \frac{2}{\exp\left(\Delta(T)/k_B T\right) + 1} \tag{6.12}$$

where $\Delta(T)$ is the temperature dependent energy band gap:

$$\Delta(T) = C \cdot \frac{k_B T_c}{\sqrt{1 - (T/T_c)}} \tag{6.13}$$

The data shown in Fig. 6.8 agree with (6.12) and the fit parameter is $C = 3.8 \pm 0.7$. That is in relatively good agreement with BCS theory established value—$C = 3.5$. Based on those data the simplified mechanism might be sketched. In the superconducting phase, the electrons lose their identity and form Cooper pairs. Therefore, the energy is lost only to the emission of phonons. The acoustic wave created by oscillating tip interacts only with the normal electrons near the Fermi surface. Close to T_C the normal electron population is gradually growing and the acoustic wave attenuation rises due to electron-phonon scattering, which causes an onset of dissipation.

Further measurements of voltage V and distance d dependent friction support the hypothesis of separation of phononic and electronic channels. In Fig. 6.9 the $\Gamma(V)$ is shown in metallic state ($T = 13\,\mathrm{K}$) and in superconducting state ($T = 5.8\,\mathrm{K}$), both acquired at the same tip sample distance $d = 0.5\,\mathrm{nm}$. In the normal state data follow a quadratic dependence $\Gamma(V) \propto V^2$, as expected for dissipation due to ohmic

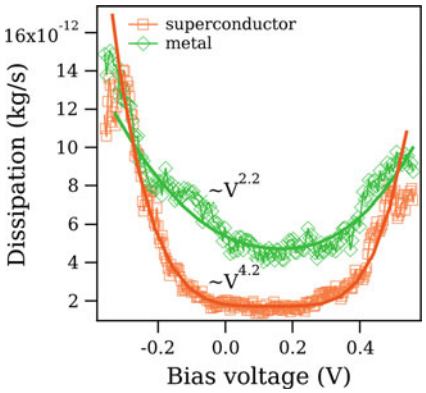

Fig. 6.9 The non-contact friction as a function of the bias voltage. The data were acquired in superconducting (*red*) and normal (*green*) state. The dissipation has a parabolic dependence in metallic state, while $\Gamma \propto \mathrm{V}^4$ for superconducting state of Nb. The tip sample distance is constant and equal $d = 0.5\,\mathrm{nm}$

looses [3, 4], In contrary to that in the superconducting state the friction depends on the fourth power of voltage—$\Gamma(V) \propto V^4$. Volokitin et al. [3, 4] calculated the non-contact friction between spherical tip oscillating laterally above the elastic surface. The friction is proportional to the second power of the static force—$\Gamma \propto F^2$. Since $F \propto V^2$, the friction coefficient has to vary as a fourth power of the voltage, which is in very good agreement with the measurement.

Dependence of the friction coefficient Γ on distance d for metallic and superconducting phase is shown in Fig. 6.10. The distance changes in between $0 < d < 3\,\mathrm{nm}$ and the contact potential is compensated. In normal state clear rise of dissipation is visible few nanometers away from the surface, otherwise as in the case of superconducting Nb state. The fit of the inverse power low function $\Gamma \propto d^{-n}$ to the experimental data gives $n = 1.0 \pm 0.1$ and $n = 3.8 \pm 0.3$, respectively for normal and superconducting state. In normal state the distance dependence is in good agreement with the results obtained by Stipe et.al ($n = 1.3$) [5]. In the case of phononic friction, Lifshitz theory of van der Waals interaction [32] predicts that elastic stress leads to a vdW force $F(d) \propto d^{-2}$. Thus the phononic friction should vary as $\Gamma_{ph} \propto d^{-4}$ and the experimental value is in excellent agreement with this prediction.

6.7 The Non-contact Friction Due to Phase Slips of the Charge Density Wave (CDW) in $NbSe_2$ Sample

So far we reported on dissipation due to linear response of the system under study. The non-contact friction in that case has a form of viscous drag. It this section we report on experiment when dissipation is produced by cycle of hysteretic processes induced in the sample by oscillating cantilever tip [7]. The measured sample is $NbSe_2$—an intercalated dichalcogenide compound with bulk charge density wave (CDW) state

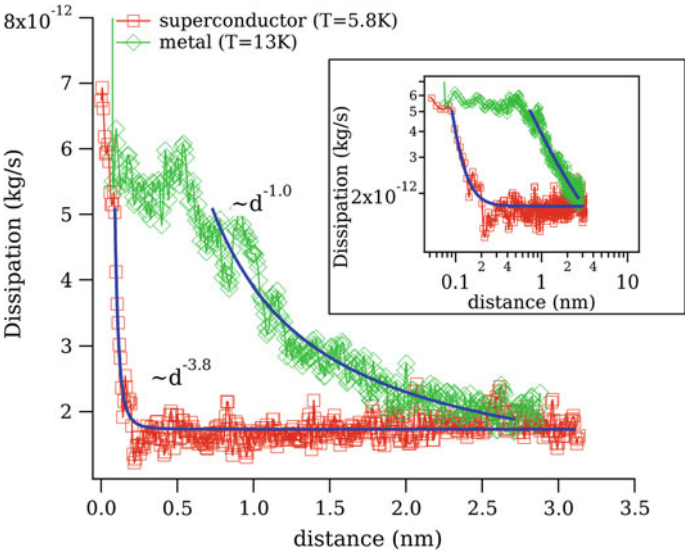

Fig. 6.10 Distance dependence of the non-contact friction coefficient for Nb superconductor (*red*) and Nb normal metal (*green*) state. The data are well fitted by inverse power law dependence $\Gamma \propto d^{-n}$ with $n = 1.0$ and $n = 3.8$, respectively for metal and superconducting state

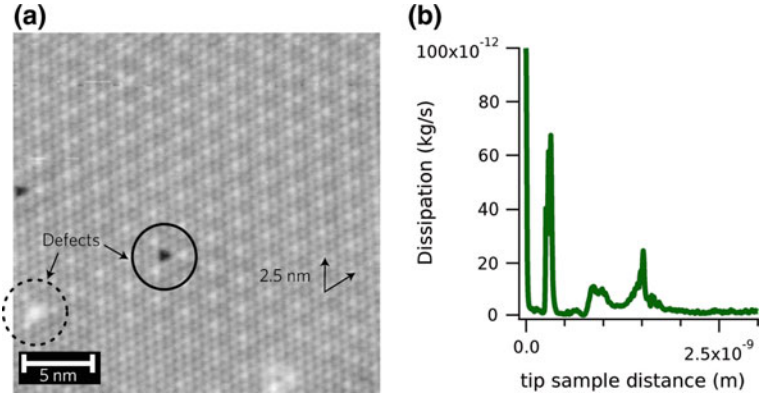

Fig. 6.11 **a** STM image of $NbSe_2$ surface obtained at $T = 6$ K. **b** The energy dissipation as a function of tip $NbSe_2$ sample distance for compensated contact potential difference. Three dissipation spikes positioned few nanometers above the surface are clearly visible

accompanied by periodic lattice distortion (PLD). Figure 6.11a shows the atomically resolved surface topography with the additional CDW induced Moirè pattern, which is incommensurate with underlying lattice. Layered dichalchogenides have long been known for their phase transitions leading to picometre-sized superstructure lattice distortions and corresponding new electronic periodicities in their low-temperature

ground state [33]. Lots of their properties, namely nonlinear conductivity, Shapiro steps are related to the CDW motion under the external voltage.

The probe consisted of a soft cantilever (ATEC-CONT from Nanosensors) with spring constant k = 120 mN/m, the resonance frequency f = 12 kHz, quality factor $Q = 9 \times 10^5$ and a friction coefficient $\Gamma_0 = 1.7 \times 10^{-12}$ kg/s (at 6 K). Due to the asymmetric tip design the cantilever lateral oscillatory motion also implies a normal action. The lateral oscillation and the corresponding normal oscillation amplitudes were equal to A = 5 nm and $A_{norm} = 180$ pm, respectively. The dissipated energy was calculated according to (6.5), meaning the recorded signal was the excitation voltage needed to maintain constant oscillation amplitude. The distance dependence of friction coefficient $\Gamma(d)$ shows striking multiple of dissipation peaks arising at few nanometer distance from the surface, as shown in Fig. 6.11b. The data are contrary to most non-contact friction experiments, where the energy dissipation increases smoothly as the tip approaches the surface [5, 6]. Here however, the train of peaks on $NbSe_2$ surface is perfectly reproducible over well ordered surfaces. Moreover, the temperature evolution of the peaks suggests a strong connection with the CDW.

The dissipated power $P(z, V)$ versus tip sample distance z and tip sample bias voltage V is shown in Fig. 6.12. The bright features correspond to high dissipation maxima up to P = 2 meV/cycle. Within each dissipation branch the amount of energy loss stays constant, independently on bias voltage V. The giant non-contact friction maxima remain even after careful compensation of the contact potential difference

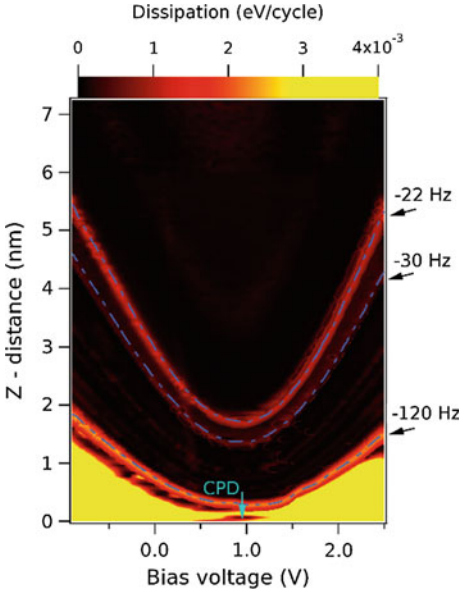

Fig. 6.12 Energy dissipation between $NbSe_2$ surface and oscillating pendulum AFM cantilever tip versus tip sample voltage and tip sample distance. Bright features correspond to high dissipation peaks. The peaks always follow the tip-sample interaction force (constant frequency shift contours $\Delta f = -22$ Hz, $\Delta f = -30$ Hz, $\Delta f = -120$ Hz are indicated with *dashed lines*)

(CPD) between the tip and the sample. In other words no matter the character of the interaction force is van der Waals ($V = V_{\mathrm{CPD}}$) or electrostatic ($V \neq V_{\mathrm{CPD}}$). Moreover, $z(V)$ dependence of the particular dissipation branch has a parabolic behaviour. For capacitively coupled conical tip and sample the force varies as $F \propto V^2/z$, meaning that the each dissipation peak always follow the same tip-sample interaction force. Indeed, the three dominant frictional maxima might be nicely superimposed with dashed lines which correspond to contours of constant cantilever frequency shift (constant conservative force)—$\Delta f = -22\,\mathrm{Hz}$, $\Delta f = -30\,\mathrm{Hz}$ and $\Delta f = -120\,\mathrm{Hz}$—as tip approaches the sample's surface. The above observations mean that the effect is force controlled rather than voltage controlled.

In order to understand the origin of dissipation spikes a theoretical model was proposed, where the CDW is considered to be an elastic medium, perturbed locally by the attractive potential of the cantilever tip [34, 35]. The CDW is described through phase $\phi(x)$ and amplitude $\rho(x)$ order parameters and the latter is assumed to be constant in case of small perturbations. Thus only phase degree of freedom is considered. The total energy is estimated according to equation:

$$E[\phi(x)] = \int [(\nabla\phi(x))^2 + V(x)\rho(x)]\mathrm{d}x. \tag{6.14}$$

Where first term is an elastic energy and the second stands for perturbation. The energy given by (6.14) is next minimized in order to find the preferential shape of the phase. This is shown in Fig. 6.13. For a given perturbation the charge peak below the tip displaces (red solid line) and the resulting CDW phase is getting distorted

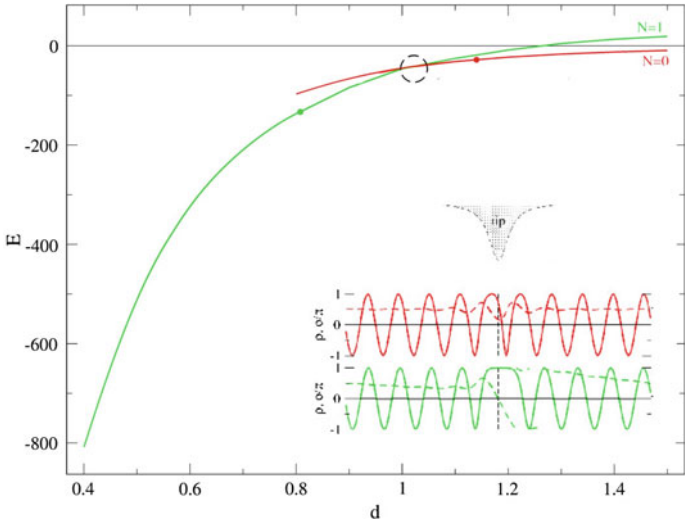

Fig. 6.13 The calculated energy E as a function of distance d for locally perturbed elastic charge density wave. The tip oscillation around crossover point (marked by a *circle*) causes hysteresis in tip dynamics. *Inset* shows the charge density (*solid lines*) and phase (*dashed lines*) of the CDW under the tip perturbation respectively for two different energy-distance curves

(red dashed line). As the force reaches critical value the central peak disappears and an extra 2π phase is pumped locally below the cantilever tip (green dashed line). The energies for the two discussed phase deformations are shown in Fig. 6.13 and a crossover energy is marked by a circle. Oscillations close to a crossover point will cause pumping *in* and *out* an extra 2π phase and thus be accompanied by a hysteresis cycle in the tip mechanics. The hysteresis explains the giant size of dissipation peaks despite the extremely low tip oscillation frequency. Approaching the tip further down, there can be another phase slip explaining multiple dissipation peaks.

More sophisticated theoretical model taking into account the other dimensions, namely y-intersurfaceplane, and z-intounderlying is presented elsewhere [36].

6.8 Conclusion

The contribution of non-contact friction to the friction force of a typical sliding contact is about one billionth. Very soft silicon sensors with high quality factors operated in pendulum geometry let us to measure those elusive friction forces. Cantilever annealing under ultra high vacuum conditions improves the force sensitivity by at least an order of magnitude. The effect is mainly due to removal of adsorbates from the cantilever surface. Cooling to cryogenic temperatures reduces the thermal fluctuations and lowers the internal friction further down. Approaching the cantilever to the surface opens new dissipation channels. At large tip-sample separations the long range Joule dissipation is dominant frictional process. Compensation of the contact potential minimizes the contribution of Joule dissipation into non-contact friction. A direct way to distinguish between electronic and phononic contribution to friction is to work across the superconducting phase transition. It was demonstrated that the non-contact friction coefficient is reduced by a factor of three when the sample enters the superconducting state. The temperature behaviour of Γ was found to be in good agreement with BCS theory of superconductivity. Thus friction has an electronic character in normal metal state, whereas the phononic friction dominates in the superconducting phase. The experiment on $NbSe_2$ surface reports on dissipation being a result of hysteresis switching induced in the sample. It was demonstrated that noncontact AFM dissipation dramatically peaks when an extra 2π phase is locally "pumped" into the phase of a charge-density-wave material surface, by the mechanical oscillation of a tip hovering above the surface at a large distance of one nanometer or more. Because states with and without the local 2π shift behave as different branches of the energy in a simple phase-only model, their crossing is expected to give rise to mechanical hysteresis, explaining the large dissipation of the peaks even at extremely low oscillation frequencies.

Acknowledgments We express our gratitude to E. Gnecco, S. Rast, L. Marot, R. Pawlak, F. Pellegrini, G.E. Santoro, R. Buzio, A. Gerbi, G. Balakrishnan, A. Baratoff and E. Tosatti for collaboration and helpful discussions. This work was supported by the Swiss National Science Foundation.

References

1. B. Gottsmann, H. Fuchs, Phys. Rev. Lett. **86**, 2597 (2001)
2. A. Vanossi, N. Manini, M. Urbakh, S. Zapperi, E. Tosatti, Rev. Mod. Phys. **85**, 529–552 (2013)
3. A. Volokitin, B. Persson, Phys. Rev. Lett. **94**, 086104 (2005)
4. A.I. Volokitin, B.N.J. Persson, H. Ueba, Phys. Rev. B **73**, 165423 (2006)
5. B.C. Stipe, H.J. Mamin, T.D. Stowe, T.W. Kenny, D. Rugar, Phys. Rev. Lett. **87**, 096801–1 (2001)
6. M. Kisiel, E. Gnecco, U. Gysin, L. Marot, S. Rast, E. Meyer, Nat. Mater. **10**, 119 (2011)
7. M. Langer, M. Kisiel, R. Pawlak, F. Pellegrini, G.E. Santoro, R. Buzio et al., Nat. Mater. **13**, 173 (2013). doi:10.1038/NMAT3836
8. G. Binnig, H. Roher, Ch. Gerber, E. Weibel, Phys. Rev. Lett. **49**, 57 (1982)
9. R. Perez, Nat. Mater. **13**, 118 (2014)
10. U. Gysin, S. Rast, M. Kisiel, C. Werle, E. Meyer, Rev. Sci. Instrum. **82**, 023705 (2011)
11. G. Meyer, N.M. Amer, Appl. Phys. Lett. **53**, 2400 (1988)
12. I. Dorofeyef, H. Fuchs, G. Wenning, B. Gotsmann, Phys. Rev. Lett. **83**, 2402 (1999)
13. W. Denk, D.W. Pohl, Appl. Phys. Lett. **59**, 2173 (1991)
14. B.C. Stipe, H.J. Mamin, T.D. Stowe, T.W. Kenny, D. Rugar, Phys. Rev. Lett. **86**, 2874 (2001)
15. S. Rast, Sensoren mit geringer Dissipation zur Messung kleiner Krafte, Diss. Phil.-naturwiss. Fak., Basel, 1999
16. J. Lübbe, L. Tröger, S. Torbrügge, R. Bechstein, C. Richter, A. Kühnle et al., Meas. Sci. Technol. **21**, 125501 (2010)
17. K.G. Lyon, G.L. Salinger, C.A. Swenson, G.K. White, J. Appl. Phys. **48**, 865 (1977)
18. H. Haucke, X. Liu, J.F. Vignola, B.H. Houston, M.H. Marcus, J.W. Baldwin, Appl. Phys. Lett. **86**, 191903 (2005)
19. J. Yang, T. Ono, M. Esashi, Appl. Phys. Lett. **77**, 3860 (2000)
20. S. Rast, U. Gysin, P. Ruff, Ch. Gerber, E. Meyer, D.W. Lee, Nanotechnology **17**, 189 (2006)
21. T. Albrecht, T.R. Albrecht, P. Grutter, H.K. Horne, D. Rugar, J. Appl. Phys. **69**, 668 (1991)
22. K. Saitoh, K. Hayashi, Y. Shibayama, K. Shirahama, Phys. Rev. Lett. **105**, 236103 (2010)
23. B. Gotsmann, Nat. Mater. **10**, 8788 (2011)
24. R. Kubo, Rep. Prog. Theor. Phys. **29**, 255 (1966)
25. R. Kubo, M. Toda, N. Hashitsume, *Statistical Physics Vol. II, Nonequlibrium Statistical Mechanics* (Springer, Berlin, 1995)
26. A.I. Volokitin, B.N.J. Persson, Solid State Commun. **115**, 145 (2008)
27. J.B. Pendry, J. Phys. Condens. Matter **9**, 10301 (1997)
28. G.V. Dedkov, Wear **232**, 145 (1999)
29. J. Bardeen, L.N. Cooper, J.R. Schrieffer, Phys. Rev. **108**, 1175 (1957)
30. B.N.J. Persson, *Sliding Friction* (Springer, Berlin, 2000)
31. B.N.J. Persson, Solid State Commun. **115**, 145 (2000)
32. R. Lifshitz, M. Roukes, Phys. Rev. B **61**, 5600 (2000)
33. C. Schlenker, *Physics and Chemistry of Low-Dimensional Inorganic Conductors*. North Atlantic Treaty Organization, & NATO Advanced Study Institute on Physics and Chemistry of Low-Dimensional Inorganic Conductors (Plenum Press, New York, 1996)
34. H. Fukuyama, P.A. Lee, Dynamics of the charge-density wave. I. Impurity pinning in a single chain. Phys. Rev. B **17**, 535–541 (1978)
35. P.A. Lee, T.M. Rice, Electric field depinning of charge density waves. Phys. Rev. B **19**, 3970–3980 (1979)
36. F. Pellegrini, G.E. Santoro, E. Tosatti, Phys. Rev. B **89**, 245416 (2014)